A planetesimal orbiting within the debris disc around a white dwarf star

Christopher J. Manser[1]*, Boris T. Gänsicke[1,2], Siegfried Eggl[3], Mark Hollands[1], Paula Izquierdo[4,5], Detlev Koester[6], John D. Landstreet[7,8], Wladimir Lyra[3,9], Thomas R. Marsh[1], Farzana Meru[1], Alexander J. Mustill[10], Pablo Rodríguez-Gil[4,5], Odette Toloza[1], Dimitri Veras[1,2], David J. Wilson[1,11], Matthew R. Burleigh[12], Melvyn B. Davies[10], Jay Farihi[13], Nicola Gentile Fusillo[1], Domitilla de Martino[14], Steven G. Parsons[15], Andreas Quirrenbach[16], Roberto Raddi[17], Sabine Reffert[16], Melania Del Santo[18], Matthias R. Schreiber[19,20], Roberto Silvotti[21], Silvia Toonen[22]†, Eva Villaver[23], Mark Wyatt[24], Siyi Xu[25], Simon Portegies Zwart[26]

Many white dwarf stars show signs of having accreted smaller bodies, implying that they may host planetary systems. A small number of these systems contain gaseous debris discs, visible through emission lines. We report a stable 123.4-minute periodic variation in the strength and shape of the Ca II emission line profiles originating from the debris disc around the white dwarf SDSS J122859.93+104032.9. We interpret this short-period signal as the signature of a solid-body planetesimal held together by its internal strength.

More than 3000 planet-hosting stars are known (*1*), the vast majority of which will end their lives as white dwarfs. Theoretical models indicate that planetary systems, including the Solar System, can survive the evolution of their host star largely intact (*2*–*4*). Remnants of planetary systems have been indirectly detected in white dwarf systems via (i) the contaminated atmospheres of 25 to 50% of white dwarfs, arising from the accretion of planetary material (*5*, *6*); (ii) compact dust discs (*7*, *8*), formed from the rubble of tidally disrupted planetesimals (*9*, *10*); and (iii) atomic emission lines from gaseous discs colocated with the circumstellar dust (*11*, *12*). The most-direct evidence for remnant planetary systems around white dwarfs is provided by transit features in the light-curve of WD 1145+017, which are thought to be produced by dust clouds released from solid planetesimals orbiting the white dwarf with a period of ≃4.5 hours (*13*, *14*). Searches for transiting debris around other white dwarfs have been unsuccessful (*15*–*17*). White dwarfs are intrinsically faint, so transit searches are limited to a lower sky density than that of main-sequence star systems. The probability of detecting transits is further limited by the narrow range of suitable orbital inclinations and the duration of a planetesimal disruption event (*18*).

The gaseous components of debris discs identified around a small number of white dwarfs enable us to probe the underlying physical properties of the discs. Double-peaked emission profiles are observed in a number of ionic transitions, such as the Ca II 850- to 866-nm triplet, indicating Keplerian rotation in a flat disc (*19*). Previous repeat observations of the gaseous debris disc at the white dwarf SDSS J122859.93+104032.9 (hereafter SDSS J1228+1040) have revealed long-term variability—on a time scale of decades—in the shape of the emission lines (*20*), indicating ongoing dynamical activity in the system.

We performed short-cadence spectroscopy (a cadence of 100 to 140 s) targeting the Ca II triplet in SDSS J1228+1040 on 20 and 21 April 2017 and again on 19 March, 10 April, and 2 May 2018. Our observations were conducted with the 10.4-m Gran Telescopio Canarias [(GTC) on La Palma, Canary Islands], with the goal of searching for additional variability on the Keplerian orbital time scales within the disc, which are on the order of hours (*21*). We detected coherent low-amplitude (≃3%) variability in the strength and shape of the Ca II triplet with a period of 123.4 ± 0.3 min (Fig. 1), which is present in all three components of the triplet after subtracting the average emission line profile for the five nights of observations (Fig. 1). Because the variability is detected in observations separated by more than a year, it has been present in the disc for ≃4400 orbital cycles. Using Kepler's third law and adopting the mass, M, of SDSS J1228 + 1040 as $M = 0.705 \pm 0.050\ M_{\odot}$ (where $1\ M_{\odot}$, the mass of the Sun, is 1.99×10^{30} kg) (*6*), the semimajor axis, a, of the orbit corresponding to the additional Ca II emission is $a = 0.73 \pm 0.02\ R_{\odot}$ (where $1\ R_{\odot}$, the radius of the Sun, is 6.96×10^{8} m).

The equivalent widths [(EWs), a measure of the strength of the lines relative to the continuum] of the Ca II triplet profiles are shown in Fig. 2 along with the ratios of blueshifted to redshifted flux throughout the 123.4-min period. This illustrates the variation in the overall brightness of the emission lines and the strong asymmetry of the velocity of the additional flux. The variable emission shown in Fig. 1, C and F, alternates (moves) from redshifted to blueshifted wavelengths as a function of phase. Assuming that the additional, variable emission is generated by gas in orbit around the white dwarf, this indicates that we observe emission only when the additional gas is on the far side of its orbit around the white dwarf, with respect to our line of sight. This additional emitting region is obscured, either by the disc or the region itself, when the material is traveling in front of the star, where we would otherwise observe the blueshifted-to-redshifted transition. We fitted sinusoids to both the EW and blue-to-red ratio data, finding them to be offset in phase by 0.14 ± 0.01 cycles and 0.09 ± 0.01 cycles in 2017 and 2018, respectively. These phase shifts imply that the maximum EW is observed when the region emitting the additional flux is at its maximum visibility and thus furthest from us in its orbit around the white dwarf, whereas the maximum blueshifted emission occurs up to 0.25 cycles afterward, once the region has orbited into the visible blueshifted quadrant of the disc. The smoothness of the EW and blue-to-red ratio variations, along with the extent in orbital phase (≃0.4) of the variable emission in Fig. 1, indicates that the emission region is extended in azimuth around the disc, rather than originating from a point source.

Several scenarios could plausibly explain the short-term emission detected from SDSS J1228+1040 (see supplementary text): (i) A low-mass companion could be found, with Ca II

[1]Department of Physics, University of Warwick, Coventry CV4 7AL, UK. [2]Centre for Exoplanets and Habitability, University of Warwick, Coventry CV4 7AL, UK. [3]Jet Propulsion Laboratory, California Institute of Technology, 4800 Oak Grove Drive, Pasadena, CA 91109, USA. [4]Instituto de Astrofísica de Canarias, E-38205 La Laguna, Tenerife, Spain. [5]Departamento de Astrofísica, Universidad de La Laguna, E-38206 La Laguna, Tenerife, Spain. [6]Institut für Theoretische Physik und Astrophysik, Universität Kiel, 24098 Kiel, Germany. [7]Department of Physics and Astronomy, The University of Western Ontario, London, Ontario, N6A 3K7, Canada. [8]Armagh Observatory and Planetarium, College Hill, Armagh, Co. Armagh BT61 9DG, UK. [9]Department of Physics and Astronomy, California State University, Northridge, 18111 Nordhoff St., Northridge, CA 91330, USA. [10]Lund Observatory, Department of Astronomy and Theoretical Physics, Lund University, Box 43, SE-221 00 Lund, Sweden. [11]McDonald Observatory, University of Texas at Austin, Austin, TX 78712, USA. [12]Department of Physics and Astronomy, Leicester Institute of Space and Earth Observation, University of Leicester, University Road, Leicester LE1 7RH, UK. [13]Physics and Astronomy, University College London, London WC1E 6BT, UK. [14]Osservatorio Astronomico di Capodimonte, National Institute for Astrophysics, Via Moiarello 16, 80131 Napoli, Italy. [15]Department of Physics and Astronomy, The University of Sheffield, Western Bank, Sheffield S10 2TN, UK. [16]Landessternwarte, Zentrum für Astronomie der Universität Heidelberg, Königstuhl 12, 69117 Heidelberg, Germany. [17]Dr. Karl Remeis-Sternwarte, Astronomisches Institut der Universität Erlangen-Nürnberg, Sternwartestr. 7, 96049, Bamberg, Germany. [18]National Institute for Astrophysics/Institute of Space Astrophysics and Cosmic Physics, via Ugo La Malfa 153, 90146, Palermo, Italy. [19]Instituto de Física y Astronomía, Universidad de Valparaíso, Av. Gran Bretaña 1111, 5030 Casilla, Valparaíso, Chile. [20]Milennium Nucleus for Planet Formation - NPF, Universidad de Valparaíso, Av. Gran Bretaña 1111, Valparaíso, Chile. [21]National Institute for Astrophysics, Osservatorio Astrofisico di Torino, Strada dell'Osservatorio 20, 10025 Pino Torinese, Italy. [22]Anton Pannekoek Instituut voor Sterrenkunde, University of Amsterdam, P.O. Box 94249, 1090 GE, Amsterdam, Netherlands. [23]Departamento de Física Teórica, Universidad Autónoma de Madrid, Cantoblanco 28049 Madrid, Spain. [24]Institute of Astronomy, Madingley Rd, Cambridge CB3 0HA, UK. [25]Gemini Observatory, Northern Operations Center, 670 N. A'ohoku Place, Hilo, HI 96720, USA. [26]Sterrewacht Leiden, Leiden University, P.O. Box 9513, 2300 RA Leiden, Netherlands.
***Corresponding author. Email: c.j.manser92@googlemail.com** †Present address: Institute for Gravitational Wave Astronomy and School of Physics and Astronomy, University of Birmingham, Birmingham B15 2TT, UK.

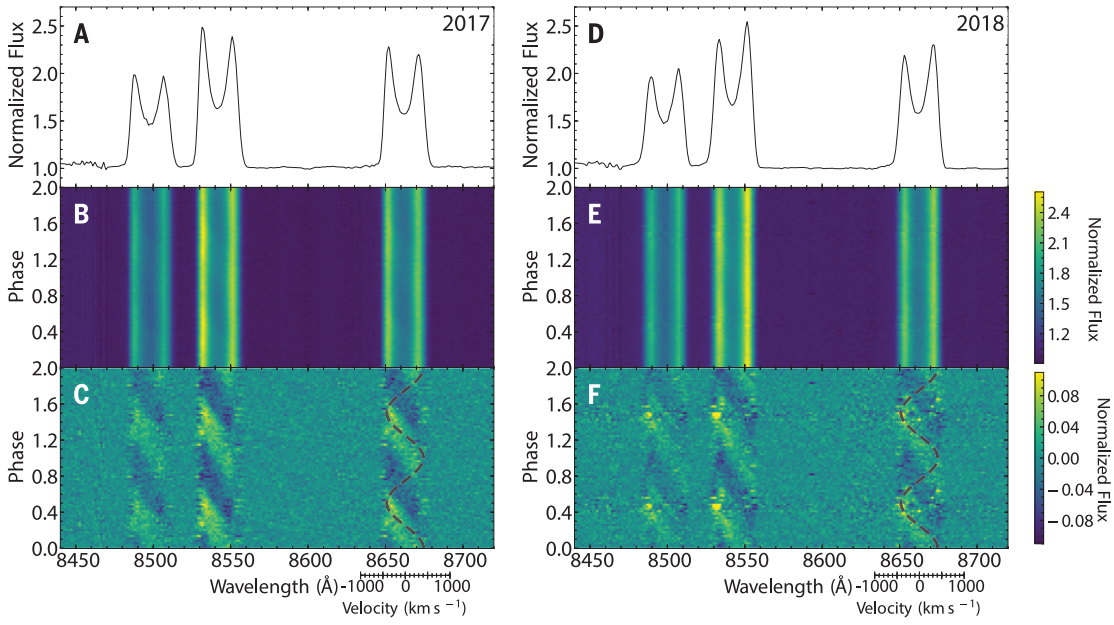

Fig. 1. Phase-folded trailed spectrogram of the emission line profiles in SDSS J1228+1040. Five hundred nineteen spectra of SDSS J1228+1040 were taken over two nights in 2017 [(A) to (C)] and three nights in 2018 [(D) to (F)]; see table S1 for a log of observations. (**A** and **D**) Averaged, normalized spectrum of the Ca II triplet. (**B** and **E**) Phase-folded trailed spectrograms using a 123.4-min period (one cycle is repeated for display). The color map represents the normalized flux. Subtracting the coadded spectrum from the phase-folded trailed spectrogram (done separately for each year) illustrates the variability in both flux and wavelength on the 123.4-min period in all three components of the Ca II triplet (**C** and **F**). The dashed black curve is not fitted to the data but simply illustrates the typical S-wave trail for a point source on a circular orbit with a semimajor axis of 0.73 $R_{\odot}$ and an inclination of 73° (*11*). The velocity axes refer to the longest-wavelength Ca II triplet line profile.

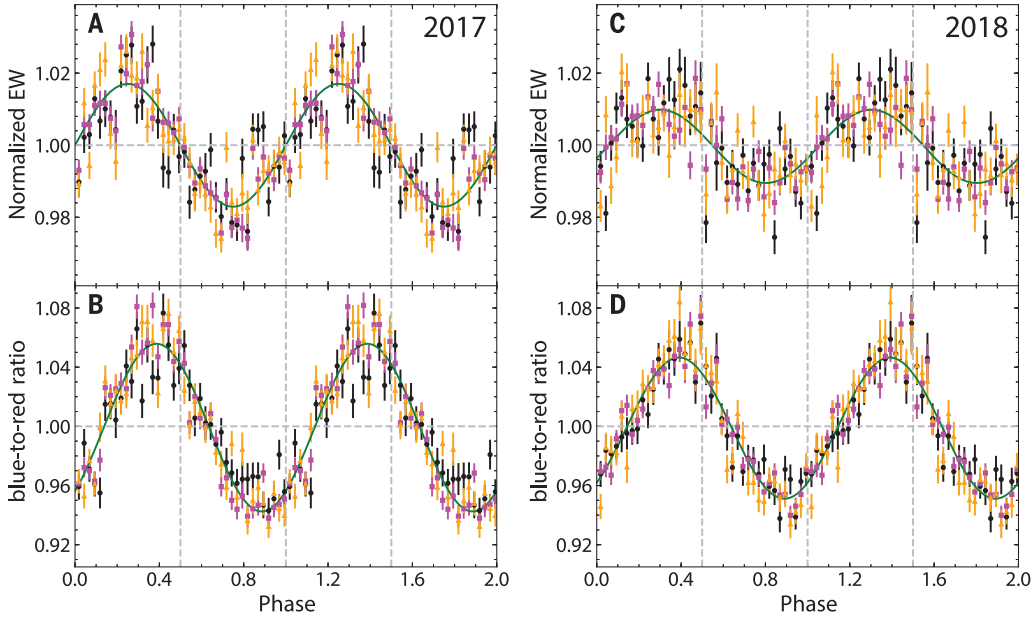

Fig. 2. Variability of the Ca II triplet emission of SDSS J1228+1040. Equivalent width (EW) (**A** and **C**) and blue-to-red ratio (**B** and **D**), which is the ratio of blueshifted to redshifted flux centered on the air wavelengths of the Ca II triplet in the rest frame of the white dwarf at +19 km s^{-1}, with the mean set to 1.0. The data are phase-folded on a 123.4-min period [one cycle repeated for clarity (*21*)] for the 2017 [(A) and (B)] and 2018 [(C) and (D)] datasets. The EWs and blue-to-red ratios for the 8498-, 8542-, and 8662-Å components of the Ca II triplet are colored (marked) in black (circles), magenta (squares), and orange (triangles), respectively. The data are averaged over the three profiles and fitted with a sinusoid (green curves). The EW and the blue-to-red ratio curves are offset in phase by 0.14 ± 0.01 cycles (49° ± 4°) and 0.09 ± 0.01 cycles (31° ± 5°) for the 2017 and 2018 profiles, respectively. Phase zero for both the 2017 and 2018 datasets has been shifted such that the fit to the 2017 EW data passes through zero at zero phase, and the vertical dashed lines denote the phases 0.5, 1.0, and 1.5. Error bars indicate the standard error of the data.

emission originating from the inner hemisphere irradiated by the white dwarf. This would naturally match the observed phase dependence (*22*). However, radial velocity measurements rule out the presence of any companion with mass greater than 7.3 M_J (where 1 M_J, the mass of Jupiter, is 1.90×10^{27} kg) (*21*), and the nondetection of hydrogen in the accretion disc excludes brown dwarfs and Jupiter-mass planets. (ii) Vortices have been invoked to explain nonaxisymmetric structures detected in submillimeter observations of protoplanetary discs (*23*). The presence of a weak magnetic field is expected to destroy any vortex that forms within a few orbital cycles. Although our observations place only an upper limit on the magnetic field of the white dwarf $B < 10$ to 15 kG (*21*), the field strength required within the disc at SDSS J1228+1040 to render vortices unstable is 10 μG to 50 mG. This field strength can be reached rapidly, owing to the exponential growth rate of the magnetic field in

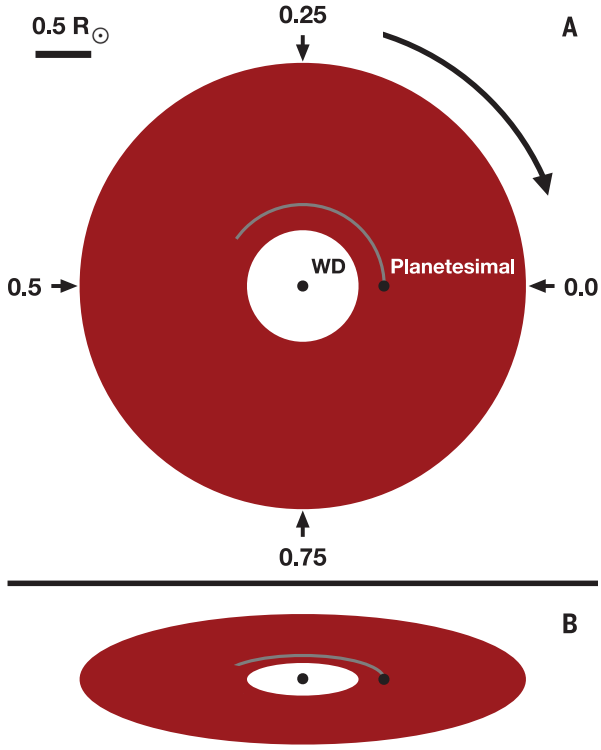

Fig. 3. Schematic for the disc structure of SDSS J1228+1040. (**A**) Top-down view of the disc around SDSS J1228+1040 with a planetesimal orbiting within the disc, assuming circular orbits. Both the disc and the planetesimal orbit clockwise, as indicated by the curved arrow. Lines of sight for specific phases from Fig. 1 are denoted by the straight arrows. The solid red region of the disc indicates the location of the observed Ca II triplet emission, and the gray curved line trailing the planetesimal shows the azimuthal extent (≃0.4 in phase) of the gas stream generating the extra emission seen in Fig. 1, C and F. WD, white dwarf. (**B**) The system at an inclination of 73°, as viewed from Earth (*11*).

the disc (*21*), and we therefore rule out the presence of long-lived vortices in the disc. (iii) The photoelectric instability (*24*) can possibly produce arc-shaped structures within a disc. However, these structures vary in both radial location and shape within the disc on the time scale of months, so we reject this scenario. (iv) A planetesimal orbiting in the disc and interacting with the dust could generate the detected gas (Fig. 3). We exclude (i) to (iii) as possible scenarios, and thus argue that (iv) is the most plausible explanation for the coherent short-term variation detected in the Ca II triplet lines at SDSS J1228+1040.

The short period of the orbit around SDSS J1228+1040 requires any planetesimal to have a high density or sufficient internal strength to avoid being tidally disrupted by the gravity of the white dwarf. By contrast, the debris fragments orbiting WD 1145+017 are detected on orbits consistent with the tidal disruption radius of a rocky asteroid (*13*). Assuming that the body in orbit around SDSS J1228+1040 has no internal strength and that its spin period is tidally locked to its orbital period, we calculate the minimum density needed to resist tidal disruption on a 123.4-min period as 39 g cm^{-3} for a fluid body deformed by the tidal forces (*21*). If the body has enough internal strength to remain spherical, then the minimum density required is reduced to 7.7 g cm^{-3}, which is approximately the density of iron at 8 g cm^{-3} (however, the internal strength could be greater and the density lower). We therefore conclude that the body in orbit around SDSS J1228+1040 needs some internal strength to avoid tidal disruption, and we calculate bounds on the planetesimal size, s, as 4 km < s < 600 km, with an uncertainty of 10% (*21*).

What is the origin of the planetesimal? This object may be the differentiated iron core of a larger body that has been stripped of its crust and mantle by the tidal forces of the white dwarf. The outer layers of such a body would be less dense and would disrupt at greater semimajor axes and longer periods than those required for core disruption (*25*). This disrupted material would then form a disc of dusty debris around SDSS J1228+1040, leaving a stripped corelike planetesimal orbiting within it.

Whether the variable emission originates from interactions with the dusty disc or from irradiation of the surface of the planetesimal remains unclear. Small bodies are known to interact with discs and induce variability in spatially resolved discs; one such object is the moon Daphnis, which produces the Keeler gap in the rings around Saturn (*26*, *27*). Some debris discs around main-sequence stars show evidence of gas generated after the main phase of planet formation (*28*). The origin of this nonprimordial gas is uncertain, but it could be generated by collisional vaporization of dust (*29*) or collisions between comets (*30*). If the body is not interacting with the disc to generate the additional gas, then the planetesimal must be producing the gas. The semimajor axis of the planetesimal, $a = 0.73\ R_{\odot}$, is close enough to the star that the surface of the body may be sublimating (*21*), releasing gas that contributes to the variable emission.

We hypothesize that gaseous components detected in a small number of other white dwarf debris discs (*11*, *31*) may also be generated by closely orbiting planetesimals. Although sublimation of the inner edges of debris discs (*32*) and the breakdown of 1- to 100-km rocky bodies (*33*) have been proposed to explain gaseous debris discs at white dwarfs, not all metal-polluted white dwarfs with high accretion rates and/or large infrared excesses host a gaseous component. The Ca II triplet emission profiles from the gaseous debris disc around SDSS J1228+1040 have shown variability over 15 years of observations [(*20*), see also Fig. 1, A and D]. This emission can be modeled as an intensity pattern, fixed in the white dwarf rest frame, that precesses with a period of ≃27 years (*20*). Both the pattern and its precession are stable for orders of magnitude longer than the orbital time scale within the disc (≃hours). Eight gaseous white dwarf debris discs are currently known; prolonged monitoring of three of these systems has shown similar long-term variability to that of SDSS J1228+1040 (*31*, *34*, *35*).

The gaseous disc has been present at SDSS J1228+1040 for at least 15 years (*20*), implying that the planetesimal has survived in its current orbit for at least that long. A planetesimal on an eccentric orbit that precesses owing to general relativity could explain the observed precession of a fixed intensity pattern. In this scenario, the planetesimal would need an eccentricity $e \simeq 0.54$ (*21*) (fig. S8), bringing the periastron to 0.34 $R_{\odot}$. An eccentric orbit is not unexpected, as the planetesimal would initially enter the tidal disruption radius at high eccentricities ($e > 0.98$) from farther out in the white dwarf system (*10*). An eccentric orbit is supported by the observed precession of an asymmetric intensity pattern in the gaseous emission (*20*). Estimating the constraints on the size of a planetesimal with such a periastron results in a range of 2 km < s < 200 km, with an uncertainty of 10%, smaller than previously calculated for a circular orbit. Our results show that planetesimals can survive in close orbits around white dwarfs, and our method is not dependent on the inclination of the disc.

REFERENCES AND NOTES

1. E. Han *et al.*, *Publ. Astron. Soc. Pac.* **126**, 827–837 (2014).
2. M. J. Duncan, J. J. Lissauer, *Icarus* **134**, 303–310 (1998).
3. E. Villaver, M. Livio, *Astrophys. J.* **661**, 1192–1201 (2007).
4. D. Veras, B. T. Gänsicke, *Mon. Not. R. Astron. Soc.* **447**, 1049–1058 (2015).
5. B. Zuckerman, C. Melis, B. Klein, D. Koester, M. Jura, *Astrophys. J.* **722**, 725–736 (2010).
6. D. Koester, B. T. Gänsicke, J. Farihi, *Astron. Astrophys.* **566**, A34 (2014).
7. B. Zuckerman, E. E. Becklin, *Nature* **330**, 138–140 (1987).
8. J. Farihi, M. Jura, B. Zuckerman, *Astrophys. J.* **694**, 805–819 (2009).
9. M. Jura, *Astrophys. J.* **584**, L91–L94 (2003).
10. D. Veras, Z. M. Leinhardt, A. Bonsor, B. T. Gänsicke, *Mon. Not. R. Astron. Soc.* **445**, 2244–2255 (2014).
11. B. T. Gänsicke, T. R. Marsh, J. Southworth, A. Rebassa-Mansergas, *Science* **314**, 1908–1910 (2006).
12. J. Guo *et al.*, *Astrophys. J.* **810**, L17 (2015).
13. A. Vanderburg *et al.*, *Nature* **526**, 546–549 (2015).
14. B. T. Gänsicke *et al.*, *Astrophys. J.* **818**, L7 (2016).
15. F. Faedi, R. G. West, M. R. Burleigh, M. R. Goad, L. Hebb, *Mon. Not. R. Astron. Soc.* **410**, 899–911 (2011).
16. C. Belardi *et al.*, *Mon. Not. R. Astron. Soc.* **462**, 2506–2517 (2016).
17. L. van Sluijs, V. Van Eylen, *Mon. Not. R. Astron. Soc.* **474**, 4603–4611 (2017).
18. J. Girven *et al.*, *Astrophys. J.* **749**, 154 (2012).
19. K. Horne, T. R. Marsh, *Mon. Not. R. Astron. Soc.* **218**, 761–773 (1986).
20. C. J. Manser *et al.*, *Mon. Not. R. Astron. Soc.* **455**, 4467–4478 (2016).
21. Materials and methods are provided as supplementary materials.
22. P. F. L. Maxted, R. Napiwotzki, P. D. Dobbie, M. R. Burleigh, *Nature* **442**, 543–545 (2006).
23. A. Isella *et al.*, *Astrophys. J.* **775**, 30 (2013).

24. H. Klahr, D. N. C. Lin, . *Astrophys. J.* **632**, 1113–1121 (2005).
25. D. Veras, P. J. Carter, Z. M. Leinhardt, B. T. Gänsicke, *Mon. Not. R. Astron. Soc.* **465**, 1008–1022 (2017).
26. C. C. Porco *et al*., *Science* **307**, 1226–1236 (2005).
27. M. S. Tiscareno, J. A. Burns, P. D. Nicholson, M. M. Hedman, C. C. Porco, *Icarus* **189**, 14–34 (2007).
28. W. R. F. Dent *et al*., *Science* **343**, 1490–1492 (2014).
29. A. Czechowski, I. Mann, *Astrophys. J.* **660**, 1541–1555 (2007).
30. B. Zuckerman, I. Song, *Astrophys. J.* **758**, 77 (2012).
31. D. J. Wilson *et al*., *Mon. Not. R. Astron. Soc.* **451**, 3237–3248 (2015).
32. B. D. Metzger, R. R. Rafikov, K. V. Bochkarev, *Mon. Not. R. Astron. Soc.* **423**, 505–528 (2012).
33. S. J. Kenyon, B. C. Bromley, *Astrophys. J.* **850**, 50 (2017).
34. C. J. Manser, B. T. Gänsicke, D. Koester, T. R. Marsh, J. Southworth, *Mon. Not. R. Astron. Soc.* **462**, 1461–1469 (2016).
35. E. Dennihy *et al*., *Astrophys. J.* **854**, 40 (2018).
36. ESO science archive, http://archive.eso.org/eso/eso_archive_main.html.
37. GTC public archive, http://gtc.sdc.cab.inta-csic.es/gtc/jsp/searchform.jsp.

ACKNOWLEDGMENTS

This work is based on observations made with the Gran Telescopio Canarias (GTC), installed in the Spanish Observatorio del Roque de los Muchachos of the Instituto de Astrofísica de Canarias, in La Palma, Canary Islands. This work has made use of data from the European Space Agency (ESA) mission *Gaia* (www.cosmos.esa.int/gaia), processed by the *Gaia* Data Processing and Analysis Consortium [(DPAC), www.cosmos.esa.int/web/gaia/dpac/consortium]. Funding for the DPAC has been provided by national institutions, in particular the institutions participating in the *Gaia* Multilateral Agreement. Based on observations made with European Southern Observatory (ESO) Telescopes at the La Silla Paranal Observatory under program IDs: 595.C-0650. **Funding:** This research has been carried out with telescope time awarded by the CCI International Time Programme. The research leading to these results has received funding from the European Research Council under the European Union's Seventh Framework Programme (FP/2007-2013)/ERC grant agreement 320964 (WDTracer). T.R.M. acknowledges support from STFC (ST/P000495/1). J.D.L acknowledges the funding support of the Natural Sciences and Engineering Research Council of Canada. D.V. acknowledges the support of the STFC via an Ernest Rutherford Fellowship (grant ST/P003850/1). M.R.S. is thankful for support from Fondecyt (1141269). A.J.M. and M.B.D. acknowledge the support of KAW project grant 2014.0017. A.J.M. also acknowledges the support of VR grant 2017-04945. O.T. was partially supported by a Leverhulme Trust Research Project Grant. F.M. acknowledges support from the Royal Society Dorothy Hodgkin Fellowship. P.R.-G. acknowledges support provided by the Spanish Ministry of Economy, Industry and Competitiveness through grant AYA-2017-83383-P, which is partly funded by the European Regional Development Fund of the European Union. This research was supported by the Jet Propulsion Laboratory through the California Institute of Technology postdoctoral fellowship program, under a contract with the National Aeronautics and Space Administration. **Author contributions:** C.J.M. led the overall project. C.J.M., B.T.G., S.E., J.D.L., W.L., A.J.M., and D.J.W. contributed to the writing of the manuscript. T.R.M., F.M., and D.V. contributed to the interpretation of the results. C.J.M., M.H., and P.I. reduced the spectra obtained from VLT/UVES and GTC/OSIRIS. D.K. and O.T. produced the white dwarf models used by J.D.L. to calculate the magnetic field strength of the white dwarf. W.L. produced the photoelectric instability simulations of the disc. P.R.-G., T.R.M., M.R.B., M.B.D., J.F., N.G.F., D.d.M., S.G.P., A.Q., R.R., S.R., M.D.S., M.R.S., R.S., S.T., E.V., M.W., S.X., and S.P.Z. contributed to the proposals that led to the data collection and discussion of the results. **Competing interests:** The authors declare no conflict of interests. **Data and materials availability:** The data used in this research are available from the ESO VLT archive (*36*), under proposal number 595.C-0650 (G), and the GTC archive (*37*), under proposal numbers GTC1–16ITP and GTC25–18A. The ZEEMAN software and the model shown in fig. S5 are available from https://sourceforge.net/projects/zeeman-f/. The PENCIL CODE software is available at https://github.com/pencil-code; we used version #f4f2f16, with the model shown in figs. S6 and S7 in the directory pencil-code/samples/2d-tests/WhiteDwarfDisk.

SUPPLEMENTARY MATERIALS

www.sciencemag.org/content/364/6435/66/suppl/DC1
Materials and Methods
Supplementary Text
Figs. S1 to S8
Tables S1 to S3
References (*38*–*113*)